# VIBRATION AND STABILITY OF PLATES USING FINITE ELEMENTS

R. G. Anderson, B. M. Irons and O. C. Zienkiewicz

University of Wales, Swansea

**Abstract**—Simple displacement functions for the flexure of triangular plate elements have proved successful in static solutions. Here the same element is used for calculating frequencies and buckling loads of plates.

Excellent accuracy is attainable in frequency calculations, and reasonably good stability predictions may be made using quite coarse element subdivisions. Numerical integration is used in deriving element properties, permitting thickness variation within an element. Some implications of this process are discussed.

Finally, a powerful "eigenvalue economizer" technique is presented which permits very fine subdivisions of elements with eigenvalue calculations of limited size.

## 1. INTRODUCTION

THE principles of the finite element method together with a large number of examples of its application have been described in many papers and have recently been dealt with fully in a text [1].

This paper is concerned with vibration and stability problems of thin plates. All the usual assumptions are made, as in classical plate theory [2]. The element chosen for the analysis is the non-conforming triangular plate bending element first described in 1965 [3]. For details of the element shape functions and its formulation, readers are referred to the text [1].

## 2. THEORY OF FREE VIBRATIONS OF PLATES

The matrix equation giving the natural frequencies $\omega$ and the modal shapes $\{\delta\}$ is

$$([K] - \omega^2[M])\{\delta\} = 0 \tag{1}$$

where $[K]$ is the sum of the stiffnesses of the individual elements and $[M]$ is the sum of the elementary mass matrices over the whole structure including any concentrated nodal masses. For computation (1) can be reduced to

$$[K]^{-1}[M]\{\delta\} = (1/\omega^2)\{\delta\}$$

but this technique is inefficient and another is recommended (equation (22) below).

If we consider the case with no concentrated masses at the nodes, $[M]$ is assembled in the usual way from the element mass matrices $[m]^e$. These, like $[k]^e$, are given in general terms in Ref. [1] or in the case of a plate bending element by

$$[m]^e = \int\int \rho[\bar{N}]^T[\bar{N}] \, dx \, dy$$

where $[\bar{N}]$ is the shape function vector, and $\rho$ is the mass per unit area of plate.

The element stiffness and mass matrices can be found explicitly. The integration is considerably easier in area co-ordinates, because a typical integral over the triangle is given [6] by

$$\iint L_1^i L_2^j L_3^k \, dx \, dy = \text{(twice area of triangle)} i!j!k!/(i+j+k+2)! \tag{2}$$

However, it is even simpler to program numerical integration (as described in the Appendix with some comments on accuracy).

## 3. THEORY OF ELASTIC STABILITY OF PLATES

The strain energy of a single plate element subject to in-plane stresses can be written as

$$V = V_B + V_s \tag{3}$$

where $V_s$ is the strain energy due to the in-plane stresses acting on the second order strains, and $V_B$ is the strain energy due to plate bending. $V_s$ can be expressed as [1, 4, 5]

$$V_s = -\frac{1}{2} \iint \left[ \sigma_x \left(\frac{\partial w}{\partial x}\right)^2 + \sigma_y \left(\frac{\partial w}{\partial y}\right)^2 + 2\tau_{xy} \frac{\partial w}{\partial x} \cdot \frac{\partial w}{\partial y} \right] t \, dx \, dy \tag{4}$$

or written in matrix form as

$$V_s = -\frac{1}{2} \iint \begin{bmatrix} \dfrac{\partial w}{\partial x} & \dfrac{\partial w}{\partial y} \end{bmatrix} \begin{bmatrix} \sigma_x & \tau_{xy} \\ \tau_{xy} & \sigma_y \end{bmatrix} \begin{bmatrix} \dfrac{\partial w}{\partial x} \\ \dfrac{\partial w}{\partial y} \end{bmatrix} t \, dx \, dy. \tag{5}$$

Now, the lateral displacement $w$ can be written as

$$w = |\bar{N}| \{\delta^e\} \tag{6}$$

where $\bar{N}$ is again the shape function vector and $\{\delta^e\}$ is a vector of nodal deflections. Writing

$$\begin{bmatrix} \dfrac{\partial w}{\partial x} \\ \dfrac{\partial w}{\partial y} \end{bmatrix} = \begin{bmatrix} \dfrac{\partial \bar{N}}{\partial x} \\ \dfrac{\partial \bar{N}}{\partial y} \end{bmatrix} \{\delta^e\} = [S]\{\delta^e\} \tag{7}$$

we have

$$V_s = -\tfrac{1}{2} \iint \{\delta^e\}^T [S]^T [\sigma] [S] \{\delta^e\} t \, dx \, dy. \tag{8}$$

On differentiating with respect to the nodal displacements this component of strain energy gives a "geometric stiffness"

$$
\begin{bmatrix}
\dfrac{\partial V^e}{\partial \delta_1} \\
\vdots \\
\dfrac{\partial V^e}{\partial \delta_N}
\end{bmatrix}
= -[k_s]^e \{\delta^e\}
\tag{9}
$$

with

$$
[k_s]^e = -\iint [S]^T [\sigma][S] t \, dx \, dy.
\tag{10}
$$

For the whole plate we assemble the element matrices:

$$
([K_B] - [K_s])\{\delta\} = \{Q\}
\tag{11}
$$

where $Q$ are the generalized loads.

If all the in-plane stresses can be increased by a factor $\lambda$ this will increase the geometric stiffness proportionately. It is possible therefore to find a $\lambda$ which, with no external loading $Q$, gives

$$
([K_B] - \lambda[K_s])\{\delta\} = 0.
\tag{12}
$$

This is an eigenvalue problem like equation (1).

The geometric stiffnesses could be calculated by analytic integration from (2), but the numerical integration process is preferred.

## 4. EXAMPLES: PLATE VIBRATION—CONSTANT-THICKNESS ELEMENT

*Simple rectangular cantilever plates*

The first problem was that of a rectangular plate with constant thickness, for which tests and calculations have been done by Barton [7] and Plunkett [8].

The solutions used three different element subdivisions and the results are summarized in Table 1. Figure 1 shows the shapes of the first three modes obtained with the coarsest mesh. The accuracy is remarkable.

*Skew cantilever plates*

The plate was divided into 8 elements as in Fig. 2. Angles of skew "$\theta$" were taken as 0°, 15°, 30° and 45° and the first three modes were calculated in each case. The results are compared in Table 2 with those obtained by Barton [7] and Dawe [9]. As the angle of skew increases the results from the Ritz method evidently become less accurate, particularly for higher modes. The finite element solutions using the triangular element with a fairly coarse mesh compare favourably with those of Dawe using the parallelogram element and a much greater number of degrees of freedom.

The accuracy of the finite element method appears quite independent of the angle of skew of the plate, unlike the conventional Ritz method, and can be seen in Fig. 3 to agree closely with the corrected test results of Barton.

TABLE 1. COMPARISON BETWEEN THEORETICAL AND TEST FREQUENCIES FOR A UNIFORM THICKNESS RECTANGULAR CANTILEVER PLATE (LENGTH $a$, WIDTH $a/2$)

| | $\omega/\sqrt{(D/\rho h a^4)}$ | | | | | |
|---|---|---|---|---|---|---|
| Mode | Results from Barton | | Test results of Plunkett | Finite element (triangular non-conforming) | | |
| | Conventional Ritz method | Test | | $2 \times 1$ mesh 4 elements | $4 \times 2$ mesh 16 elements | $2 \times 8$ mesh on half plate with use of symmetry equivalent to 64 elements |
| 1 | 3·47 | 3·42* | 3·50 | 3·39 | 3·44 | 3·44 (s) |
| 2 | 14·93 | 14·52* | 14·50 | 15·30 | 14·76 | 14·77 (a) |
| 3 | 21·26 | 20·86 | 21·70 | 21·16 | 21·60 | 21·50 (s) |
| 4 | 48·71 | 46·90 | 48·10 | 49·47 | 48·28 | 48·19 (a) |
| 5 | | | 60·50 | 67·46 | 60·56 | 60·54 (s) |
| 6 | | | 92·30 | | 88·84 | 91·79 (s) |
| 7 | 94·49 | 93·99 | 92·80 | | 92·24 | 92·78 (a) |
| 8 | | | 118·70 | | 117·72 | 119.34 (s) |
| 9 | | | 125·10 | | 118·96 | 124·23 (s) |
| 10 | | | 154·00 | | | 153·15 (a) |
| 11 | | | 176·00 | | | 174·46 (s) |
| 12 | | | 196·00 | | | 199·61 (s) |

Results* have been modified by Barton to correct for the means of testing used by him. (s) denotes symmetrical mode; (a) antisymmetrical mode.
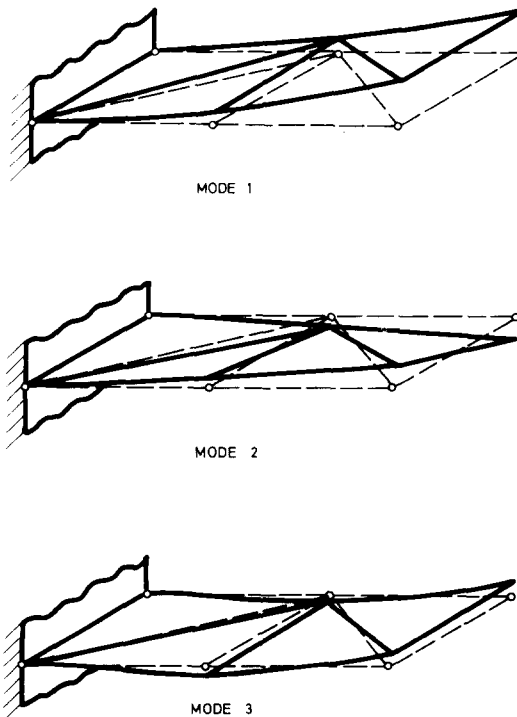


MODE 1

MODE 2

MODE 3

FIG. 1. Vibration of a cantilever plate (4 elements) modal shapes.

TABLE 2. COMPARISON BETWEEN THEORETICAL AND TEST FREQUENCIES FOR SKEW CANTILEVER PLATES

| Angle of skew $\theta°$ | Mode | Results by Barton | | | Finite element results by Dawe using parallelogram element | Finite element results triangular element |
|---|---|---|---|---|---|---|
| | | Conventional Ritz method | Test | Corrected Test | 16 elements 75 degrees of freedom | 8 elements 18 degrees of freedom |
| 0° | 1 | 3·49 | 3·37 | 3·43 | 3·47 | 3·43 |
| | 2 | 8·55 | 8·26 | 8·32 | 8·52 | 8·61 |
| | 3 | 21·44 | 20·55 | | 21·54 | 21·5 |
| 15° | 1 | 3·60 | 3·38 | 3·44 | 3·59 | 3·57 |
| | 2 | 8·87 | 8·63 | 8·68 | 8·71 | 8·60 |
| | 3 | | 21·49 | | 21·59 | 21·75 |
| 30° | 1 | 3·96 | 3·82 | 3·88 | 3·95 | 3·98 |
| | 2 | 10·19 | 9·23 | 9·33 | 9·42 | 9·19 |
| | 3 | | 24·51 | | 25·56 | 24·56 |
| 45° | 1 | 4·82 | 4·26 | 4·33 | 4·59 | 4·67 |
| | 2 | 13·75 | 11·07 | 11·21 | 11·14 | 11·01 |
| | 3 | | 26·52 | | 27·48 | 27·56 |

The table header also shows $\omega/\sqrt{(D/\rho ha^4)}$ spanning the results columns.
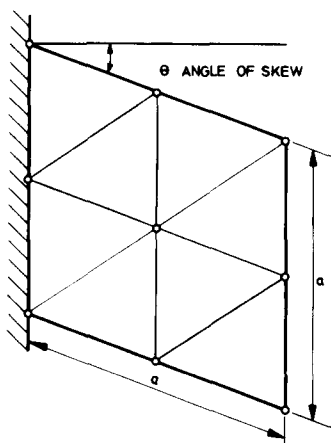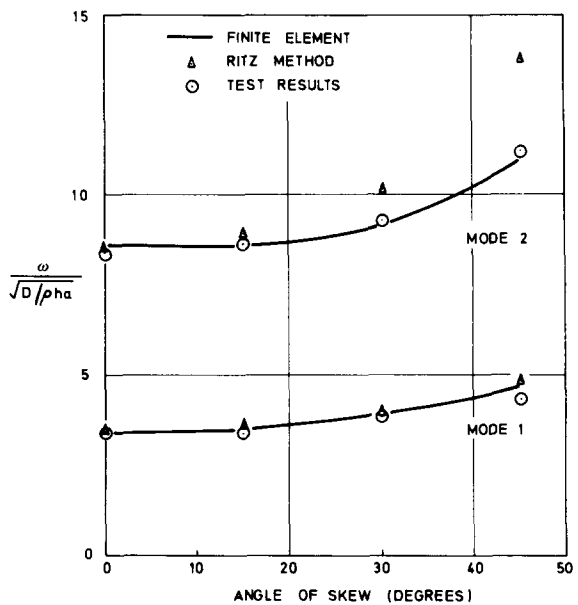


FIG. 2. Skew plate (8 elements).



FIG. 3. Frequency of vibration of skew cantilever plates.

## Plates with arbitrary boundaries

The freedom given by the triangular element to deal with arbitrary shaped plates is perhaps not evident from the previous examples, which were used for test purposes only.

While practical calculations have recently been done for variable thickness buttress dams [10] few suitable test examples are available.
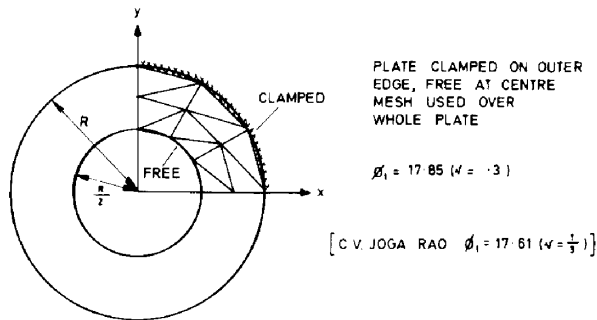
However, a clamped circular plate with a concentric hole, tested by Joga Rao [11] gives comparative results again in good agreement (see Fig. 4).

Figure 5 and Table 3 show results for square clamped plates with central circular holes of varying diameter. No test results are available for these cases.

Table 3. Frequencies of square clamped plate with circular hole

| Diameter hole $2R/a$ | $\omega/\sqrt{(D/\rho a^4 t)}$ | |
|---|---|---|
| | $\phi_1$ | $\phi_4$ |
| 0 | 35·375 | 130·540 |
| 0·125 | 35·138 | 128·637 |
| 0·25 | 37·600 | 125·464 |
| 0·3333 | 41·419 | 123·275 |
| 0·375 | 44·240 | 122·020 |
| 0·5 | 57·844 | 124·308 |

$\phi_1$ is nondimensional frequency of first mode.
$\phi_4$ is nondimensional frequency of fourth mode.



$$\phi = \frac{\omega}{\sqrt{D/\rho a^4 t}}$$

PLATE CLAMPED ON OUTER EDGE, FREE AT CENTRE MESH USED OVER WHOLE PLATE

$\phi_1 = 17·85 \; (\nu = ·3)$

$\left[ \text{C.V. JOGA RAO} \quad \phi_1 = 17·61 \; (\nu = \tfrac{1}{3}) \right]$

PLATE SIMPLY SUPPORTED ON OUTER EDGE, FREE AT CENTRE. MESH USED ON ¼ PLATE WITH CONDITIONS OF SYMMETRY

$\phi_1 = 4·99 \; (\nu = ·3)$
$\phi_4 = 22·37$

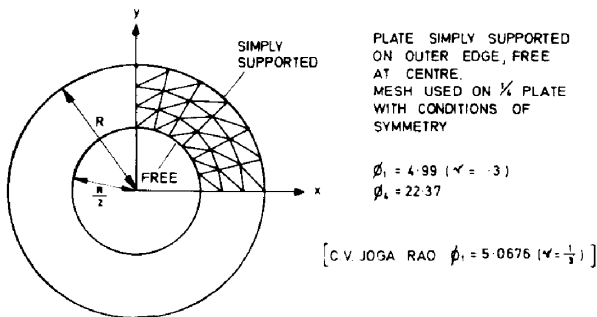$\left[ \text{C.V. JOGA RAO} \quad \phi_1 = 5·0676 \; (\nu = \tfrac{1}{3}) \right]$

Fig. 4. Circular plates with concentric holes of half the radius of the plate.
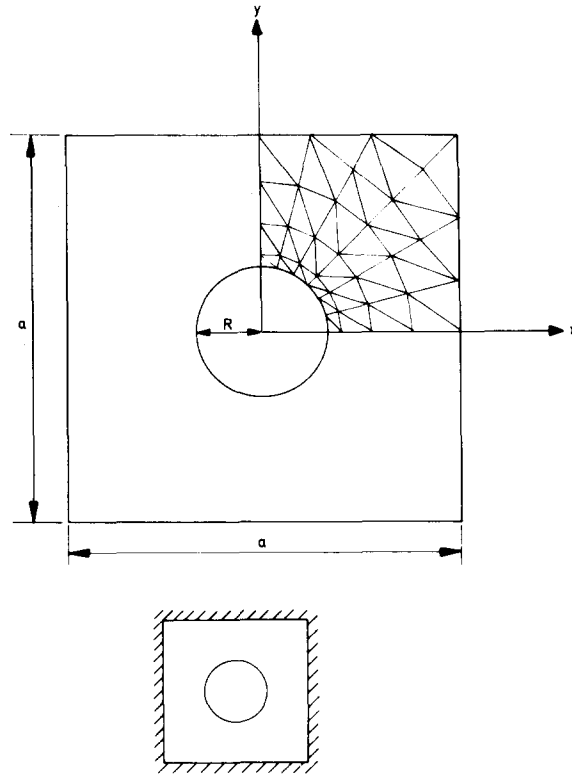
FIG. 5. Square plate with hole showing mesh used to solve quarter plate.

## 5. EXAMPLES: PLATE VIBRATION—VARIABLE-THICKNESS ELEMENTS

The usual technique with a variable thickness plate is to average the thickness of the plate over an element, and to consider each element as being of constant thickness. Theoretically one can introduce the thickness "$t$" into the formulation of the mass and stiffness matrices as a function of the $x$ and $y$ co-ordinates. However, even if "$t$" is only a linear function of $x$ and $y$ the integrals for the mass and stiffness matrices are complicated. If, however, numerical integration is used no difficulties arise. The only disadvantage is that one might need a higher order integration formula than for a constant-thickness element.

*Comparison between constant- and variable-thickness elements for a variable-thickness cantilever*

The case chosen to compare constant- and variable-thickness elements was a rectangular cantilever, divided into a regular $3 \times 6$ mesh as shown in Fig. 6. The finite element results are compared with the experimental results of Plunkett [8] in Table 4. In general the results for the variable-thickness elements agree better with experiment than those of the constant-thickness elements, particularly in the higher modes.

TABLE 4

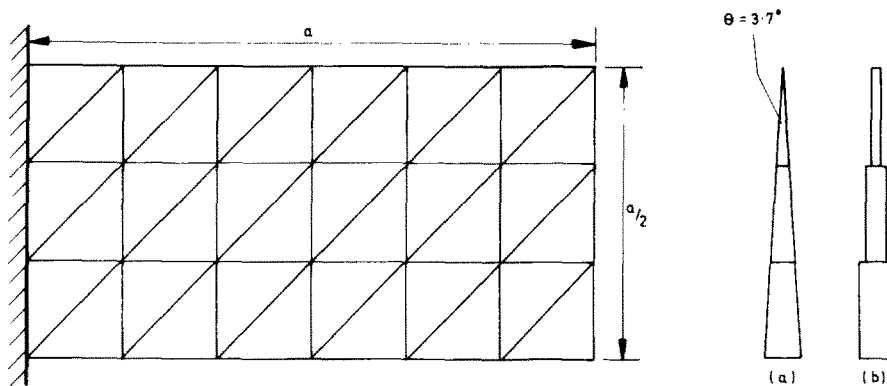| | | Finite element | |
| Mode | Test results of Plunkett | Variable thickness element (a) | Constant thickness element (b) |
|---|---|---|---|
| 1 | 2·47 | 2·40 | 2·33 |
| 2 | 10·6 | 11·27 | 10·02 |
| 3 | 14·5 | 15·14 | 14·07 |
| 4 | 28·7 | 29·41 | 21·20 |
| 5 | 34·4 | 37·30 | 26·27 |
| 6 | 47·4 | 48·99 | 27·05 |
| 7 | 52·5 | 54·87 | 37·05 |
| 8 | 54·0 | 56·67 | 42·41 |
| 9 | 63·5 | 68·06 | 48·13 |
| 10 | 68·0 | 71·30 | 51·40 |
| 11 | 85·7 | 83·73 | 67·47 |
| 12 | 91·1 | 87·74 | 71·32 |

$\omega/\sqrt{(D/\rho t a^4)}$



FIG. 6. Finite element mesh division of wedge section rectangular cantilever plate.

*Comparison of the finite difference and finite element methods in the solution of variable-thickness plates*

The square variable-thickness plate shown in Fig. 7 was tested and solved using finite differences by Basova Raju [12] for two cases of variable thickness, and both for simply supported and for encastered edges. The finite difference solution was carried out for various mesh sizes and the results were extrapolated to find the values given for an infinite mesh. The finite element solution used a 5 × 5 mesh on a quarter-plate, with variable thickness elements, and the results are tabulated in Table 5. The finite element results are good, in most cases lying between the test results and those extrapolated for an infinite mesh in the finite difference solution.
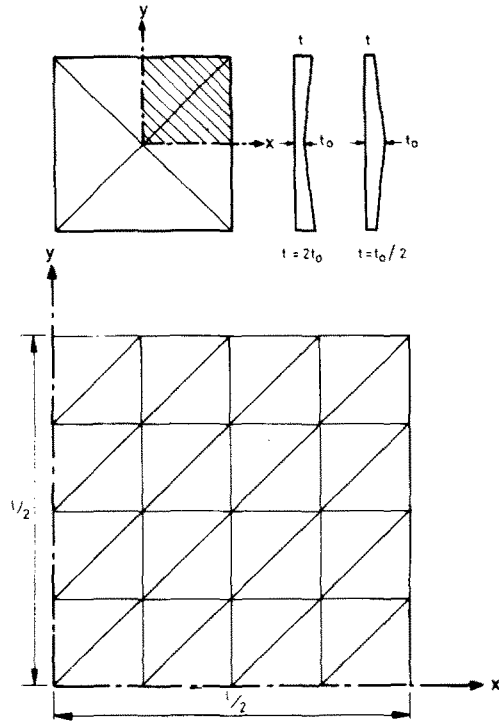
FIG. 7. Mesh for the vibration problems of a square plate of variable thickness (variable thickness element used). Results to be compared with the finite difference results of B. Basava Raju.
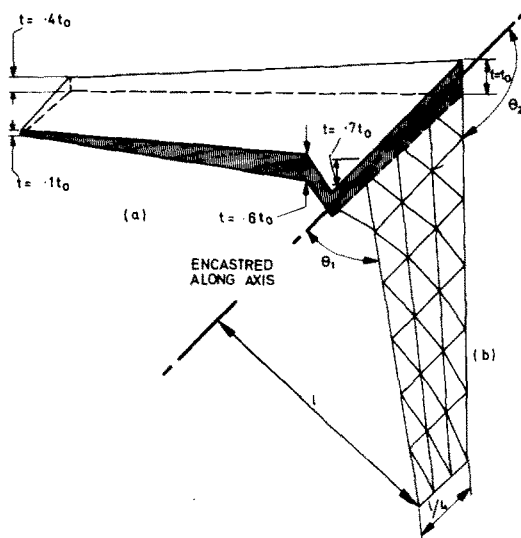


FIG. 8. Swept back cantilever plate of variable thickness: (a) isometric view, (b) element.

TABLE 5. NATURAL FREQUENCIES $(\omega/\sqrt{(D/\rho t a^4)})$

| | | Clamped plate | | | | | | Simply supported plate | | | |
|---|---|---|---|---|---|---|---|---|---|---|---|
| | | Results of B. Basava Raju | | | | | | Results of B. Basava Raju | | | |
| | | Finite difference | | Test | Finite element | | | Finite difference | | Test | Finite element |
| Model | Mode | (a) | (b) | | | Model | | (a) | (b) | | |
| Model A $t_{edge} = 2t_{centre}$ | 1 | 61·534 | 63·790 | 63·20 | 63·28 | Model D $t = 2t_0$ | | 31·431 | 32·196 | 32·84 | 32·33 |
| | 2 | 111·64 | 120·392 | 116·70 | 119·26 | | | 75·263 | 78·809 | 80·03 | 78·42 |
| | 3 | 161·688 | 178·385 | 172·20 | 171·26 | | | 122·163 | 121·544 | 128·63 | 126·43 |
| | 4 | 171·846 | 190·745 | 200·48 | 208·3 | | | 134·064 | 138·754 | 139·55 | 153·26 |
| | 5 | 174·234 | 204·199 | 201·55 | 208·5 | | | 136·759 | 152·549 | 145·85 | 157·01 |
| | 6 | 229·199 | 259·918 | 258·57 | 258·66 | | | 189·524 | 207·523 | | 203·44 |
| Model B $t_{edge} = t_{centre}$ | 1 | 19·399 | 20·936 | 21·58 | 21·40 | Model E $t = t_0/2$ | | 13·567 | 13·568 | 14·20 | 13·36 |
| | 2 | 39·541 | 43·584 | 46·54 | 45·92 | | | 32·169 | 33·195 | 34·78 | 32·74 |
| | 3 | 60·165 | 67·604 | 70·28 | 67·52 | | | 50·587 | 52·279 | 53·97 | 51·00 |
| | 4 | 67·936 | 77·749 | 87·00 | 85·45 | | | 60·771 | 66·121 | 68·16 | 67·00 |
| | 5 | 70·33 | 80·139 | | 88·08 | | | 62·816 | 68·001 | 70·93 | 67·00 |
| | 6 | 85·45 | 95·848 | 107·96 | 102·49 | | | 77·685 | 83·339 | | 81·23 |

Finite difference (a) using same mesh as finite element solutions; (b) extrapolating to get values of infinite mesh.
Finite element solutions use variable thickness element.

*A variable thickness swept-back cantilever*

   To demonstrate further the versatility of the finite element method, the swept-back cantilever shown in Fig. 8 was analysed. The frequencies and modal shapes are given in Fig. 9.
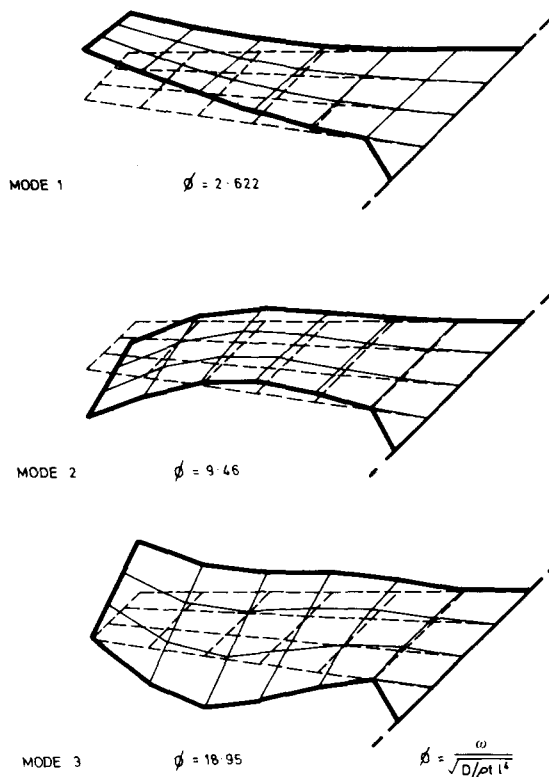
MODE 1                    $\emptyset = 2 \cdot 622$

MODE 2                    $\emptyset = 9 \cdot 46$

MODE 3          $\emptyset = 18 \cdot 95$          $\emptyset = \dfrac{\omega}{\sqrt{D/\rho t \, l^4}}$

FIG. 9. Modal shapes of swept back cantilever plate.

## 6. EXAMPLES: BUCKLING STABILITY PROBLEM

   The object of this section is to apply the theory to stability problems. The case chosen for this purpose was a simply supported square plate under uniform stress in one direction only. The meshes are shown in Fig. 10. Evidently, to obtain answers of high accuracy a very fine mesh is required. This is confirmed by the results of Kapur and Hartz [4]. (It appears that their rectangular element gives slightly better answers for the same mesh size than the triangular element. This is to be expected, as the rectangular element is of slightly higher order.)

   Other examples from finite element buckling analyses of plates are shown in Figs. 11 and 12, but the accuracy is limited by the relatively coarse meshes used.

   The conclusions reached are therefore that to obtain answers of accuracy 1 % or less a fine mesh is required. For accurate *and* economic results the eigenvalue "economizer" techniques described later in this paper are needed.
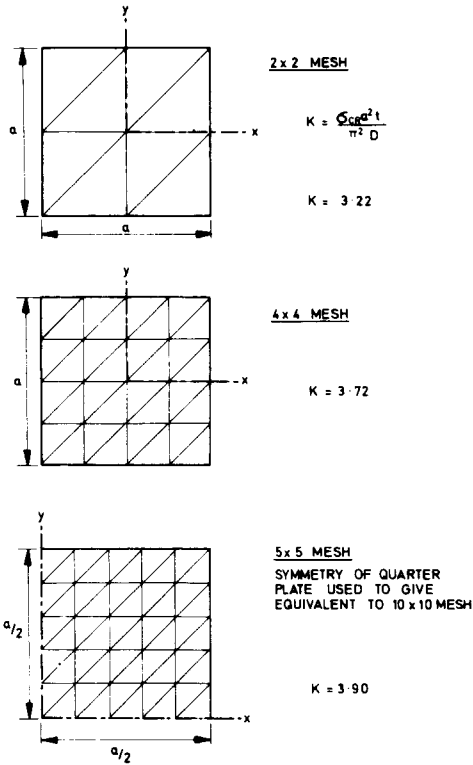
**2 x 2 MESH**

$$K = \frac{\sigma_{CR} a^2 t}{\pi^2 D}$$

$K = 3.22$

**4 x 4 MESH**

$K = 3.72$

**5 x 5 MESH**
SYMMETRY OF QUARTER
PLATE USED TO GIVE
EQUIVALENT TO 10 x 10 MESH

$K = 3.90$

FIG. 10. Stability of a simply supported plate under a uniform stress in one direction (exact $K = 4.0$).

$$K = \frac{\sigma_{yCR} a^2 t}{\pi^2 D}$$

$K_{EXACT} = 10.07$

$K = 9.30$

$K = 9.75$
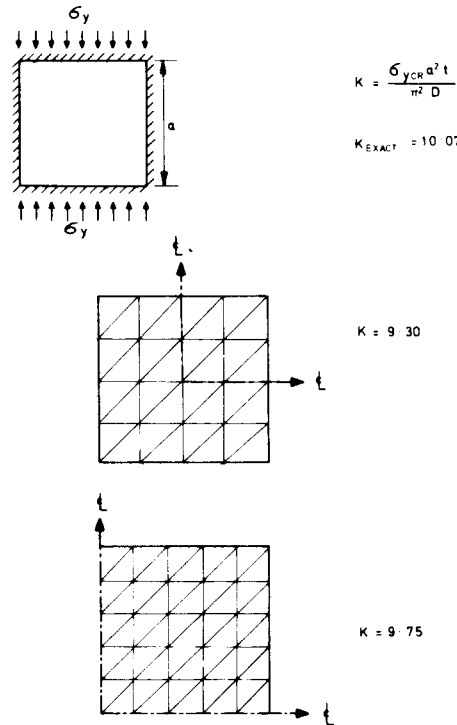
FIG. 11. Stability of clamped plate under a uniform stress in one direction.

$$K = \frac{\sigma_{yCR} a^2 t}{\pi^2 D}$$

$K_{EXACT} = 5.33$ (REF. TIMOSHENKO)
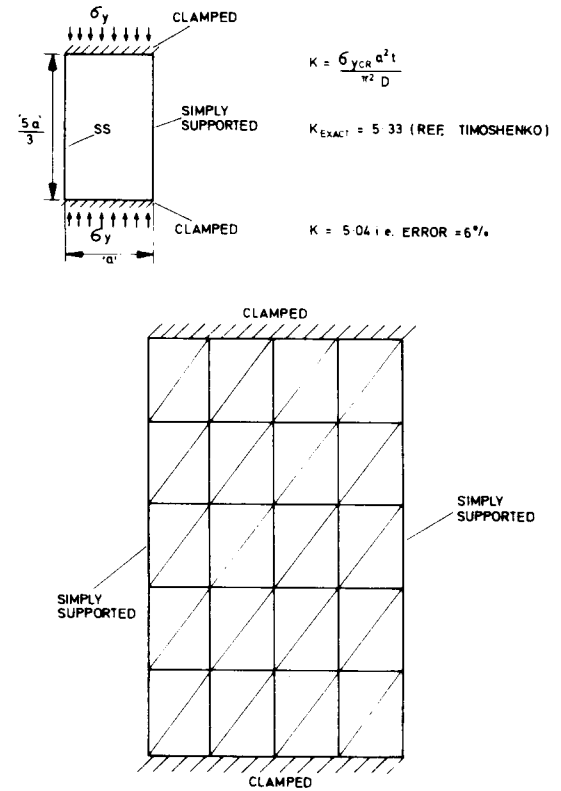
$K = 5.04$ i.e. ERROR = 6%

FIG. 12. Buckling of rectangular plate with adjacent edges pinned and clamped.

## 7. EXAMPLES: STABILITY OF A PERFORATED PLATE

A series of experimental tests were carried out at Swansea [13] to determine the buckling in shear of square clamped plates with central holes. Initially, plane plates were used with variable diameter holes, and later a constant diameter plate was tested with a variable stiffness flange around the hole. Finite element calculations were used to verify the experimental results.
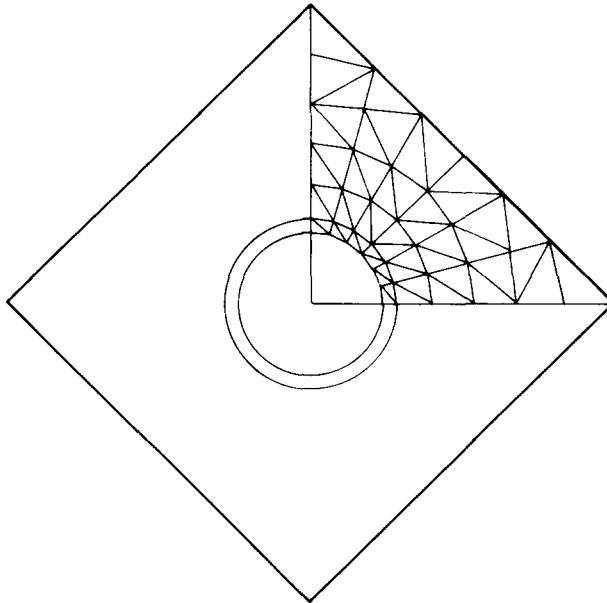


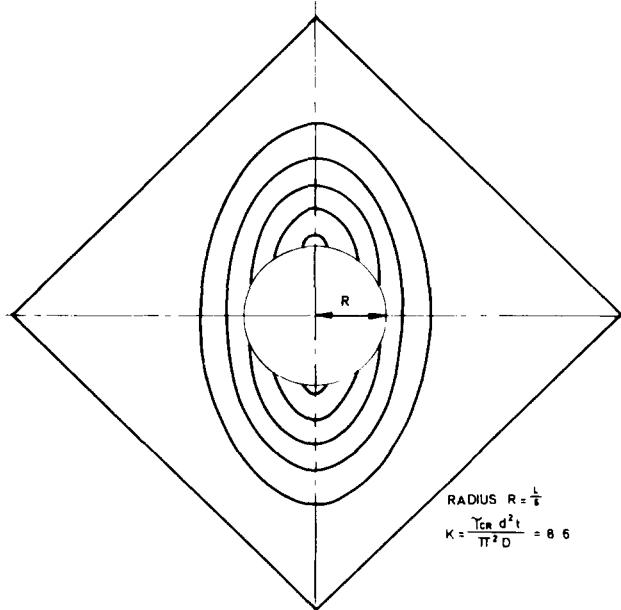FIG. 13. Square plate with hole showing mesh used.



RADIUS $R = \frac{L}{8}$

$K = \frac{\tau_{CR} \, d^2 t}{\pi^2 D} = 8 \cdot 6$

FIG. 14. Buckling mode of square clamped plate with central hole.

$$K = \frac{\gamma_{CR}\, d^2 t}{\pi^2 D} = 26\cdot12$$

FLANGE  DIMENSIONS

$$W = \frac{L}{30}, \quad t = 4t_0$$
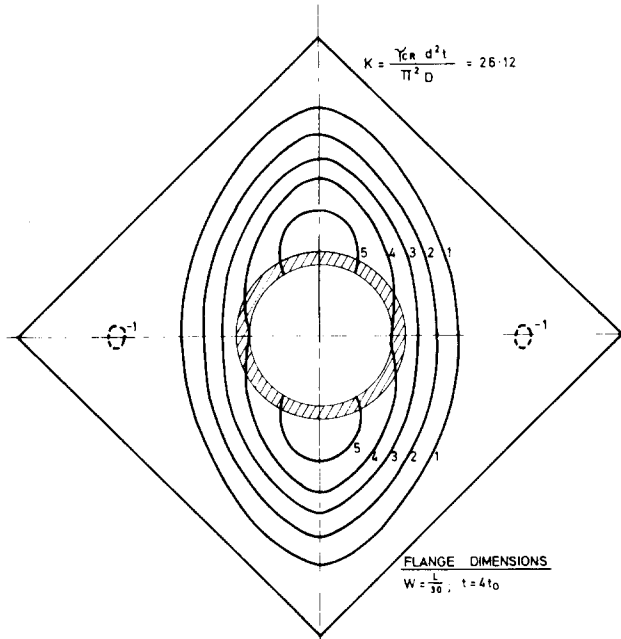
FIG. 15. Buckling mode of square plate under shear—clamped edges, central hole stiffened by flange.

DIAMETER

$$k = \frac{\gamma_{cr}\, d^3 t}{\pi^2 D}$$
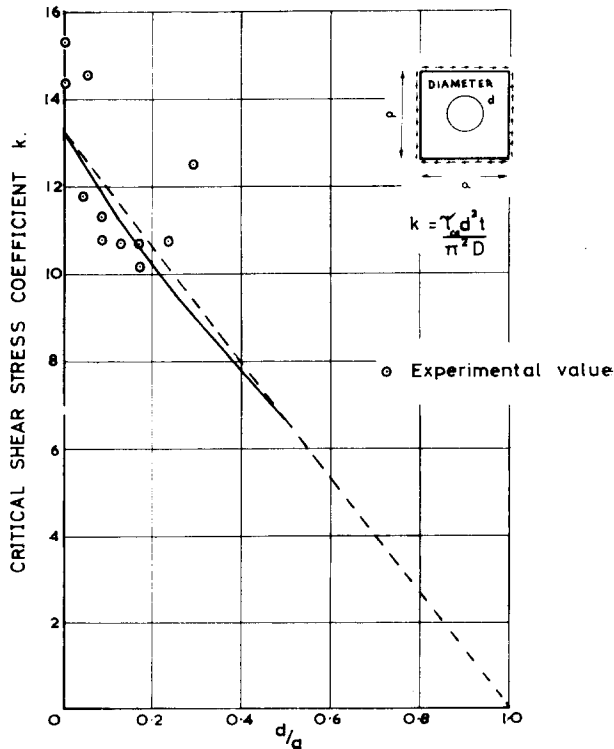
⊙ Experimental value

FIG. 16. Comparison of experimental and computed values of $k$ for a square clamped plate with a hole under uniform shear.

The mesh illustrated in Fig. 13 gave 92 degrees of freedom, and the answer for the plate without a hole was in error by 8%. This is partly due to the fact that a 1% unsymmetrical loading was applied to avoid numerical difficulties, and partly due to the coarse mesh. A mesh of equal-sized elements gave better results but was unsuitable for the plate with a hole. The initial stress distribution over the plate was found with a triangular finite element plane stress programme. Figure 16 compares some computed and experimental buckling loads.

## 8. ELIMINATION OF VARIABLES

The engineer frequently has structural problems of hundreds, or even thousands, of degrees of freedom. The eigenvalue solutions of full matrices however are very expensive, and even with only a hundred degrees of freedom they may use a great deal of computer time and storage. Clearly a technique is needed to eliminate variables, so as to reduce the number of degrees of freedom in dynamic structural problems. (See Guyan [14], and Irons [15].) It transpires that the technique is equally applicable to stability problems, although it will now be developed for vibration problems only; in stability problems the kinetic energy terms are replaced by the second order strain energy terms.

The technique used here retains only a small proportion of the nodal deflections, here-after termed "masters". The remaining "slave" deflections take the values giving least strain energy, regardless of what effect this has on the kinetic energy. Thus a slave node is assumed free from inertial forces in the vibration problem, and the deflected shape is assumed to be a linear combination of the deformation vectors due to unit loads applied for each master deflection in turn.

Given some engineering skill in choosing the master deflections, and given a problem for which point loads do not give strong local displacements, very little accuracy may be lost. The number of master nodes may be only 10% of the total, and only one deflection out of three may be retained at each, yet the frequencies may be exact for practical purposes. However, experience does suggest that there should be at least twenty master deflections. Such success may be ascribed to Rayleigh's principle, that a first-order error in modal shape gives only a second-order error in estimated frequency. When satisfactory results are obtained the suppressed degrees of freedom correspond to high frequencies, a fact which could benefit time-response calculations because it is the highest frequencies that first cause numerical instability. Conversely however it is possible to suppress or falsify the lower frequencies if inappropriate displacements are eliminated. (See below.)

The reduction is carried out simultaneously in both the mass and stiffness matrices, which occupy the same $(N + 1) \times N$ array in storage. In the frontal technique the reduction process alternates with the assembly of elements [15] according to input data which tells the program to eliminate certain deflections immediately, to turn them into slaves. Clearly the storage demands can be very small.

A typical operation is now described algebraically. The strain energy of an $N$ degree of freedom system is written as

$$\frac{1}{2}[x_1 x_2 \ldots x_N] \quad [K] \quad \begin{bmatrix} x_1 \\ \vdots \\ x_N \end{bmatrix} \tag{13}$$

and the kinetic energy as

$$\frac{\omega^2}{2g}[x_1 x_2 \ldots x_N] \quad [M] \quad \begin{bmatrix} x_1 \\ \cdot \\ \cdot \\ \cdot \\ x_N \end{bmatrix} \tag{14}$$

The condition that minimizes the strain energy with respect to $x_s$ is:

$$K_{s1}x_1 + \ldots + K_{ss}x_s + \ldots + K_{sn}x_N = 0. \tag{15}$$

Substituting for $x_s$ in (13) gives a reduced form $[K]^*$, with row and column $s$ deleted and with

$$K_{ij}^* = K_{ij} - K_{is}(K_{js}/K_{ss}). \tag{16}$$

Similarly $[M]$ becomes $[M]^*$ with

$$M_{ij}^* = M_{ij} - M_{is}(K_{js}/K_{ss}) - M_{js}(K_{is}/K_{ss}) + M_{ss}(K_{is}/K_{ss})(K_{js}/K_{ss}). \tag{17}$$

For computation the process is further simplified thus:

$$V_1^T = [K_{1s}, K_{2s} \ldots K_{Ns}] \tag{18}$$

$$V_2^T = -(M_{ss}/K_{ss})V_1^T + [M_{1s}, M_{2s} \ldots M_{Ns}] \tag{19}$$

$$[K]^* = [K] - K_{ss}^{-1}[V_1 V_1^T] \tag{20}$$

$$[M]^* = [M] - K_{ss}^{-1}[V_1 V_2^T + V_2 V_1^T] \tag{21}$$

apart from row and column $s$ in both $[K]^*$ and $[M]^*$ which must be deleted. The frontal process operates correctly as long as all the $M_{is}$ and $K_{is}$ for the row $s$ are fully summed as in equation (1).

Eigenvalues are found by power iteration using the same $(N+1) \times N$ array and associated vectors. With over-writing (1) is reduced to the form

$$[Z]\delta^* = (1/\omega^2)\delta^*$$

$$[Z] = [L]^{-1}[M][U]^{-1}$$

with

$$\delta^* = U\delta \tag{22}$$

where

$$[K] = [L][U]$$

$$[U] = [L^T] = \text{upper triangular matrix.}$$

This process is as necessary as elimination in economizing core storage.

An interesting theorem extends the conclusion that elimination must increase the lowest frequency and reduce the highest. Consider the effect of a single elimination that restricts the freedom of $x_s$, and consider how the constraint could be simulated given a leverage system that merely senses any departure from the constraint, any disobedience of the slave, and converts it into a separate linear movement. If this agitates a mass, which is progressively increased, each frequency decreases, as may be argued by computing the

Rayleigh quotient at each mass increment. Conversely if it distorts a spring each frequency increases. Complete slavery is imposed either by a heavy mass or by a stiff spring, so the new frequencies must in general interlace the old, although in theory certain frequencies could remain unchanged.

Suppose now that an $N$ degree of freedom system has been reduced to $n$ degrees of freedom by creating $(N - n)$ slaves, so that interlacing occurs at each step. It follows that within the range of the first $k$ frequencies of the original system there cannot be more than $(k - 1)$ frequencies of the reduced system. This theorem, mis-stated in Ref. [15], usually implies interlacing in practice, because otherwise a frequency in the range of interest has been inadvertently suppressed.

(a) *Vibration problems with elimination*

The square cantilever plate shown in Fig. 17 was used for initial testing. It was divided into a $5 \times 5$ mesh, giving 90 degrees of freedom, and various patterns of elimination were tried. The results are instructive.

Using elimination, one can deal with a complex structure containing well over 300 nodes, with a relatively small computer such as the University College of Swansea I.C.T. 1905. To demonstrate this a rectangular cantilever plate was divided into a $12 \times 24$ mesh, giving 576 elements and 350 nodes. The system shown in Fig. 18 contains 936 degrees of
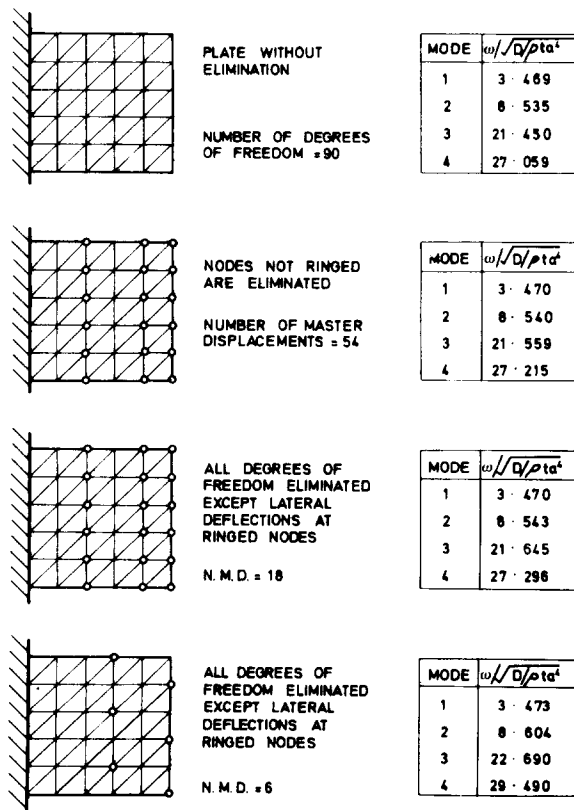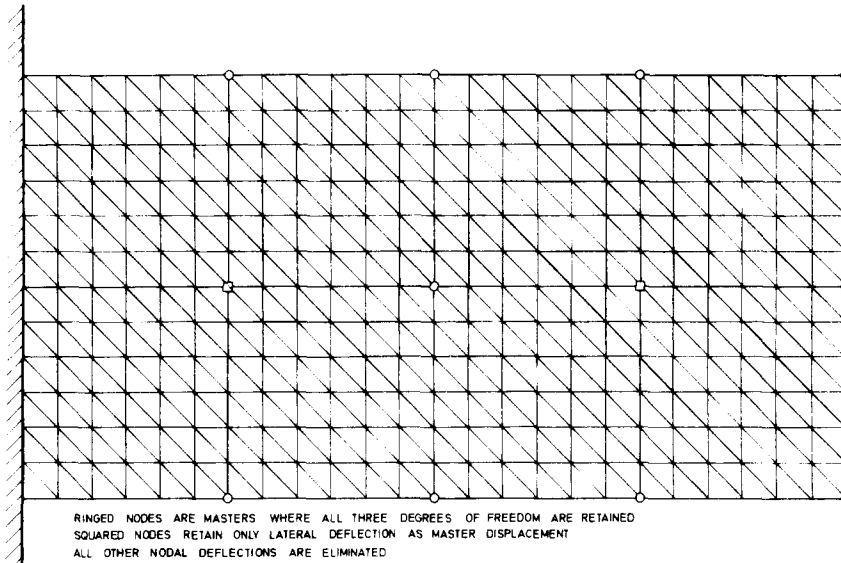
| MODE | $\omega/\sqrt{D/\rho t a^4}$ |
|------|------|
| 1 | 3·469 |
| 2 | 8·535 |
| 3 | 21·450 |
| 4 | 27·059 |

PLATE WITHOUT ELIMINATION

NUMBER OF DEGREES OF FREEDOM = 90

| MODE | $\omega/\sqrt{D/\rho t a^4}$ |
|------|------|
| 1 | 3·470 |
| 2 | 8·540 |
| 3 | 21·559 |
| 4 | 27·215 |

NODES NOT RINGED ARE ELIMINATED

NUMBER OF MASTER DISPLACEMENTS = 54

| MODE | $\omega/\sqrt{D/\rho t a^4}$ |
|------|------|
| 1 | 3·470 |
| 2 | 8·543 |
| 3 | 21·645 |
| 4 | 27·296 |

ALL DEGREES OF FREEDOM ELIMINATED EXCEPT LATERAL DEFLECTIONS AT RINGED NODES

N. M. D. = 18

| MODE | $\omega/\sqrt{D/\rho t a^4}$ |
|------|------|
| 1 | 3·473 |
| 2 | 8·604 |
| 3 | 22·690 |
| 4 | 29·490 |

ALL DEGREES OF FREEDOM ELIMINATED EXCEPT LATERAL DEFLECTIONS AT RINGED NODES

N. M. D. = 6

FIG. 17. Elimination of variables in the vibration problem of a square cantilever plate.

RINGED NODES ARE MASTERS WHERE ALL THREE DEGREES OF FREEDOM ARE RETAINED
SQUARED NODES RETAIN ONLY LATERAL DEFLECTION AS MASTER DISPLACEMENT
ALL OTHER NODAL DEFLECTIONS ARE ELIMINATED

FIG. 18. Division of rectangular cantilever plate into $12 \times 24$ mesh.

freedom, but after elimination only 32 master deflections are left. The results for the first 5 modes of vibration as given in Table 6 agree well with known results. The entire calculation was core-contained and the dimensioned arrays totalled 11,500 storage locations.

TABLE 6. THE NON-DIMENSIONAL FREQUENCIES OBTAINED
FOR A RECTANGULAR CANTILEVER PLATE DIVIDED INTO
A $12 \times 24$ MESH

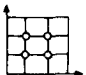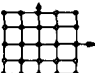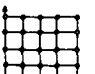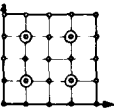| Mode | $\phi = \omega/\sqrt{(D/\rho h a^4)}$ | |
|------|-------------------|----------------------------|
|      | Finite element | Conventional Ritz method |
| 1 | 3·4403 | 3·472 |
| 2 | 14·8322 | 14·93 |
| 3 | 21·5393 | 21·61 |
| 4 | 49·1961 | 48·71 |
| 5 | 61·9205 | |
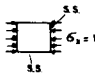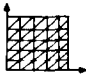
The initial problem contains 936 degrees of freedom which by elimination as shown in Fig. 18. are reduced to 32.

### (b) Stability problems

It can be seen from results quoted earlier that stability problems require considerably more nodal points than vibration problems to yield answers of similar accuracy, and elimination therefore appears to be of more potential use in civil engineering for stability problems. Without elimination the largest problem possible on the I.C.T. 1905 computer contains only 92 degrees of freedom. Thus for a simply supported square plate under

uniform stress in one direction the finest division possible is a $5 \times 5$ mesh on a quarter plate (using symmetry), giving an error of 2·5%. With elimination a finer mesh can be used, giving more accurate answers, and examples are quoted in Table 7.

TABLE 7. COMPARISON OF THE BUCKLING FACTOR CALCULATED
FOR A SQUARE SIMPLY SUPPORTED PLATE USING ELIMINATION
OF VARIABLES

| Sketch | Mesh size | $K = \dfrac{\sigma_{CR}a^2 t}{\pi^2 D}$ |
|---|---|---|
| | Exact solution | 4·00 |
| | $5 \times 5$ mesh on a quarter plate No elimination | 3·90 |
| | $3 \times 3$ mesh on a quarter plate eliminated leaving only masters of lateral deflection at circled nodes | 3·60 |
| | $8 \times 8$ mesh on whole plate reduced to masters on $4 \times 4$ mesh | 3·94 |
| | $8 \times 8$ mesh on a quarter plate elimination to masters on $4 \times 4$ mesh | 3·97 |
| | $12 \times 12$ mesh on a quarter plate eliminated to leave masters on $4 \times 4$ mesh where circled nodes are left with lateral deflection only | 3·98 |

# 9. THE EFFECT OF IN-PLANE STRESS UPON THE VIBRATION OF A THIN PLATE

The effect of any in-plane compressive stress on a plate is to reduce its bending stiffness. Similarly an in-plane tensile stress effectively increases the stiffness. Thus in the first case the natural frequency of the plate is lowered and in the second raised.

The equation for the frequencies is again as given in equation (1) but when an in-plane stress acts on the plate, $[K]$ becomes the bending stiffness of the plate $[K_B]$ less the stiffness due to in-plane stresses $[K_s]$. Thus equation (1) becomes

$$\{[K_B] - [K_s] - \omega^2[M]\}\{\delta\} = 0 \tag{23}$$

where $[K_B]$, $[K_s]$, and $[M]$ are found as before, and equation (23) is solved as in previous vibration problems.

To ensure accurate results, the solution included elimination of variables. The case chosen was a square plate simply supported around its edges, with a variable in-plane stress in one direction. Only the nodes indicated in Fig. 19 remained after elimination.

The buckling stress of the plate was determined, and then a series of vibration analyses were carried out to determine the natural frequency of the plate under in-plane stresses expressed as a fraction of the buckling stress. The results are given in Table 8 and Fig. 20, which shows that as the in-plane stress approaches the buckling stress the (frequency)$^2$ of the plate decreases linearly to zero.

TABLE 8. FREQUENCY OF SQUARE PLATE UNDER UNIFORM LOAD IN ONE DIRECTION GIVEN AS % OF BUCKLING LOAD

| Load as % of $K_{crit}$ | $\phi_1$ | $\phi_2$ | $\phi_3$ | $\phi_4$ | $\phi_1^2$ |
|---|---|---|---|---|---|
| −200 | 34·150 | 57·046 | 76·1619 | 99·33 | 1166·2 |
| −100 | 27·811 | 53·333 | 63·995 | 89·698 | 773·5 |
| −50 | 24·048 | 51·38 | 57·093 | 84·56 | 578·3 |
| 0 | 19·596 | 49·154 | 49·584 | 79·165 | 384·0 |
| 20 | 17·508 | 45·944 | 48·560 | 76·92 | 306·5 |
| 40 | 15·139 | 42·299 | 47·708 | 74·619 | 229·2 |
| 60 | 12·331 | 38·333 | 46·860 | 72·259 | 152·1 |
| 80 | 8·661 | 33·938 | 45·977 | 69·832 | 75·0 |
| 90 | 6·046 | 31·526 | 45·535 | 68·591 | 36·6 |
| 95 | 3·7046 | 30·175 | 45·154 | 67·135 | 13·7 |
| 97·5 | 2·7836 | 29·594 | 45·202 | 67·649 | 7·7 |
| 99 | 1·4096 | 29·193 | 45·134 | 67·458 | 2·0 |



$$K = \frac{\sigma_{CR} a^2 t}{\pi^2 D} = 3·97$$

$$K_{EXACT} = 4·0$$

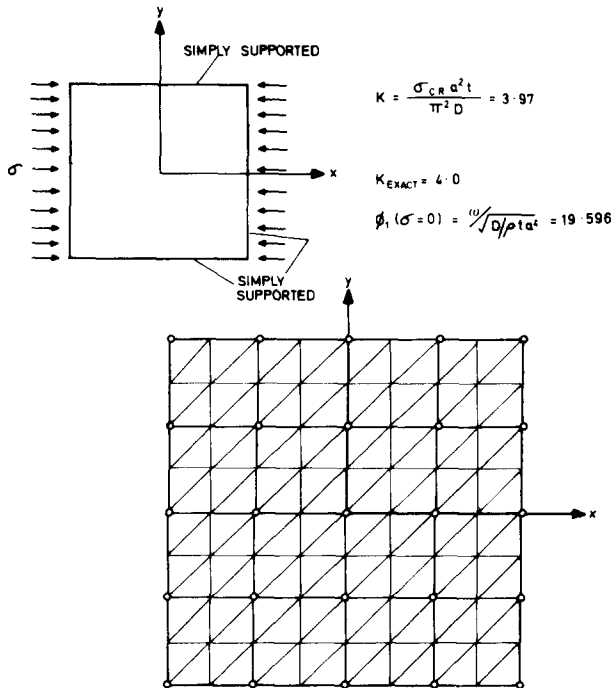$$\phi_1 (\sigma = 0) = \frac{\omega}{\sqrt{D/\rho t a^4}} = 19·596$$

FIG. 19. Mesh used to investigate the effect of in-plate stresses on the vibration of a simply supported plate.
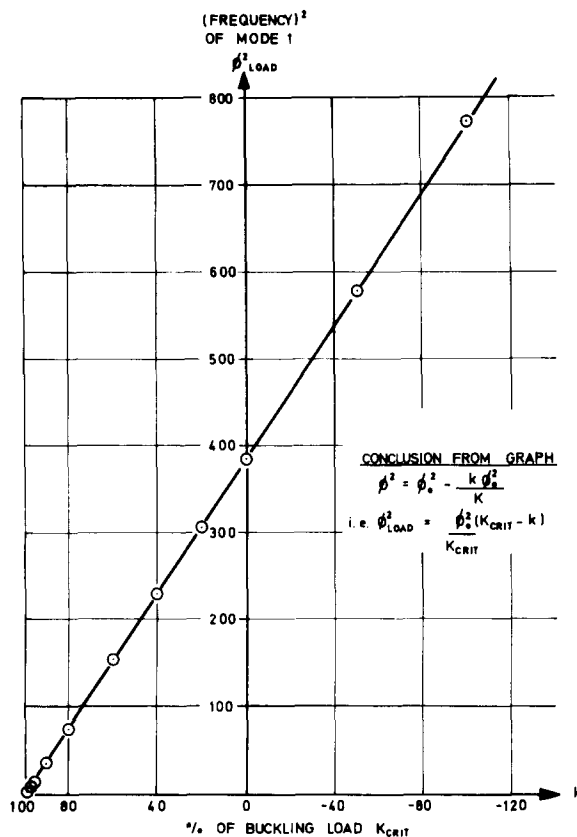
FIG. 20. Graph of frequency squared (of first mode) against percentage of buckling load applied.

# REFERENCES

[1] O. C. ZIENKIEWICZ and Y. K. CHEUNG, *The Finite Element Method of Structural and Continuum Mechanics.* McGraw-Hill (1967).

[2] S. TIMOSHENKO and S. WOINOWSKY KRIEGER, *Theory of Plates and Shells*, 2nd edition. McGraw-Hill (1959).

[3] C. B. BAZELEY, Y. K. CHEUNG, B. M. IRONS and O. C. ZIENKIEWICZ, Triangular elements on plate bending —conforming and non-conforming solutions. *Proc. Conf. on Matrix Methods in Structural Mechanics*, Air Force Inst. Tech. Wright-Patterson Air Force Base, Ohio, Oct. 1965.

[4] K. K. KAPUR and B. J. HARTZ, Stability of plates using the finite element method. *J. Engng Mech. Div. Am. Soc. civ. Engrs* (April 1966).

[5] S. F. BORG, *Matrix-Tensor Methods in Continuum Mechanics*. Van Nostrand (1963).

[6] B. M. IRONS, Algebraic integration for stiffness and flexibilities. Unpublished 3.12.62.

[7] M. V. BARTON, Vibration of rectangular and skew cantilever plates. *J. appl. Mech.* **18**, 129–134 (1951).

[8] R. PLUNKETT, Natural frequencies of uniform and non-uniform rectangular cantilever plates. *J. Mech. Engng Sci.* **5**, 146–156 (1963).

[9] D. J. DAWE, Parallelogrammic elements in the solution of rhombic cantilever plate problems. *J. Strain Analysis* **1**, No. 3 (1966).

[10] O. C. ZIENKIEWICZ, R. G. ANDERSON and B. M. IRONS, Vibration and stability of buttress dams by finite elements with particular reference to earthquake loads. *Wat. Pwr* **19**, 359–362 (1967).

[11] C. V. JOGA RAO and G. PICKETT, Vibration of plates of irregular shapes and plates with holes. *J. aeronaut. Soc. India* **13**, 83–88 (1961).

[12] B. B. RAJU, Vibration of thin elastic plates of variable thickness. *Int. J. mech. Sci.* **8**, 89–100 (1966).

[13] K. C. ROCKEY, R. G. ANDERSON and Y. K. CHEUNG, The behaviour of square shear webs having a circular hole. *Symp. on Thin Walled Steel Structures*, University College of Swansea, September 1967.
[14] R. J. GUYAN, Reduction of stiffness and mass matrices. *AIAA Jnl* **3**, 380 (1965).
[15] B. M. IRONS, Structural eigenvalue problems—elimination of unwanted variables. *AIAA Jnl* **3**, 961 (1965).
[16] B. M. IRONS, Engineering applications of numerical integration in stiffness methods. *AIAA Jnl* **4**, 2035–2037 (1966).

# APPENDIX

# NUMERICAL INTEGRATION IN AREA CO-ORDINATES

*The method*

In deriving stiffness, mass, stability and other element matrices, integrals of the form

$$\int\int \phi(L_1 L_2 L_3)\, d\,(\text{area}) \tag{A1}$$

arise frequently, where $\phi$ is a known function and the integration is taken over the triangle. The area co-ordinates define a point $P$ by ratios, so that in Fig. A1

$$L_1 = \frac{\text{area }(P23)}{\text{area }(123)} = \frac{\text{area }(P23)}{\Delta}$$

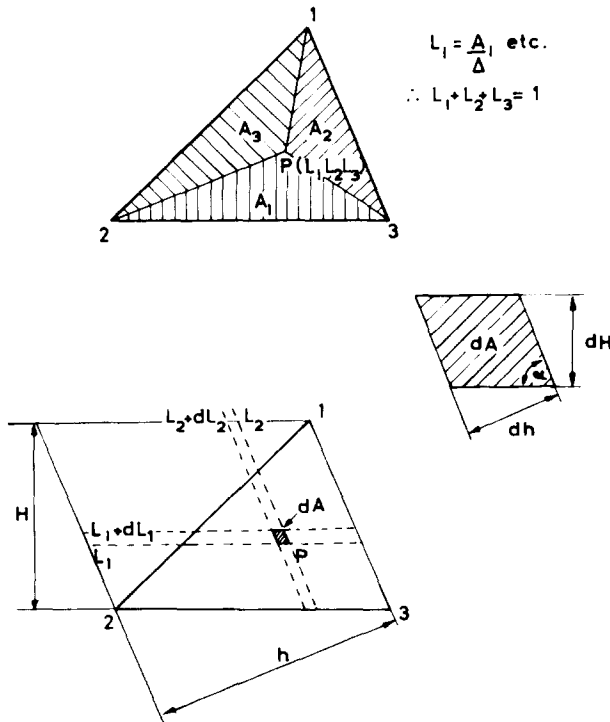The co-ordinates are thus not independent and

$$L_1 + L_2 + L_3 = 1$$



FIG. A1. Integration over a triangle.

An elementary area defined by lines incrementing $L_1$ and $L_2$ as in Fig. A1 is

$$\text{d (area)} = \frac{\mathrm{d}h \cdot \mathrm{d}H}{\cos \alpha} = \frac{h \, \mathrm{d}L_2 \cdot H \, \mathrm{d}L_1}{\cos \alpha} = \mathrm{d}L_1 \, \mathrm{d}L_2 \, 2\Delta.$$

Noting the limits of integration the integral (A1) can be written as

$$2\Delta \int_{L_1 = 0}^{L_1 = 1} \int_{L_2 = 0}^{L_2 = 1 - L_1} \phi(L_1, L_2, L_3) \, \mathrm{d}L_1 \, \mathrm{d}L_2.$$

In numerical integration the integrals are replaced by summations using "$n$" Gauss or Radau sampling points in each direction [16]. The double integral therefore becomes

$$\iint \phi \, \mathrm{d (area)} = \sum_{i=1}^{n} \sum_{j=1}^{n} N\phi(L_1, L_2, L_3)$$

where the weighting factor

$$N = 2AS[i]H[j](1 - L_1) \, \Delta$$

with

$$L_1 = AI[i]$$
$$L_2 = AJ[j](1 - L_1)$$
$$L_3 = 1 - L_1 - L_2$$

throughout. The constants for various values of $n$ are given in Table A1.

TABLE A1. GAUSS AND RADAU INTEGRATING CONSTANTS

| Number of integrating points in each direction | $AJ[J]$ $J = 1, n$ | $H[J]$ $J = 1, n$ | $AI[I]$ $I = 1, n$ | $AS[I]$ $I = 1, n$ |
|---|---|---|---|---|
| $n = 1$ | 0·5 | 1·0 | 0·3333333333 (1·0) | 0·75 (0·25) |
| $n = 2$ | 0·2113248654 | 0·5 | 0·1550510257 | 0·3764030627 |
|  | 0·7886751346 | 0·5 | 0·6449489743 (1·0) | 0·5124858262 (0·1111111111) |
| $n = 3$ | 0·1127016654 | 0·2777777778 | 0·0885879595 | 0·2204622112 |
|  | 0·5 | 0·4444444444 | 0·4094668644 | 0·3881934688 |
|  | 0·8872983346 | 0·2777777778 | 0·7876594618 (1·0) | 0·3288443200 (0·0625) |
| $n = 4$ | 0·0694318442 | 0·1739274226 | 0·0571041961 | 0·1437135608 |
|  | 0·3300094782 | 0·3260725774 | 0·2768430136 | 0·2813560151 |
|  | 0·6699905218 | 0·3260725774 | 0·5835904324 | 0·3118265230 |
|  | 0·9305681558 | 0·1739274226 | 0·8602401357 (1·0) | 0·2231039011 (0·04) |
| $n = 5$ | 0·0469100770 | 0·1184634425 | 0·0398098571 | 0·1007941926 |
|  | 0·2307653449 | 0·2393143353 | 0·1980134179 | 0·2084506672 |
|  | 0·5 | 0·2844444444 | 0·4379748102 | 0·2604633916 |
|  | 0·7692346551 | 0·2393143353 | 0·6954642734 | 0·2426935942 |
|  | 0·9530899230 | 0·1184634425 | 0·9014649142 (1·0) | 0·1598203766 (0·277777778) |

*The accuracy*

In most problems four point integration rules were used ($n = 4$), and the results were of course indistinguishable from those where the matrices were integrated analytically. Further, the computer times were unchanged, so that no penalty was paid for a device which makes the programmes simpler and sidesteps the tedious algebra.

It is important to investigate whether fewer integrating points could give adequate and convergent solutions. As elements get smaller, the variation of the displacements, slopes and curvatures decreases and it might appear that in the limit a single-point Gaussian integration would suffice. Indeed, convergence can be demonstrated with one-point integration, by arguments following Ref. [3], addendum.

An example given in Fig. A2, with numerical results in Table A2, concerns the vibration of a square cantilever plate; frequencies are compared using mesh subdivisions and four integration rules. Even with the finest mesh the one-point integration gives poor results, but the $2 \times 2$ rule is almost adequate. Little is gained by going above the $3 \times 3$ integration process.



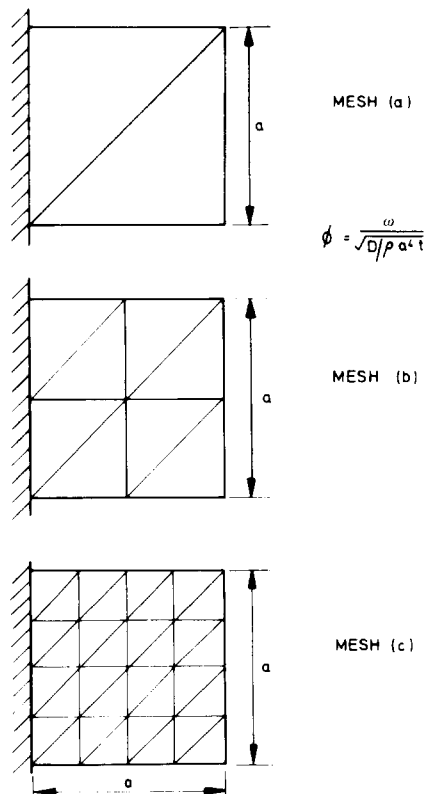$$\phi = \frac{\omega}{\sqrt{D/\rho \, a^4 \, t}}$$

Fig. A2. Meshes used on cantilevered plates to investigate the numerical integration of elemental mass and stiffness matrices.

TABLE A2. FREQUENCIES CALCULATED FOR CANTILEVER PLATE SHOWN USING GAUSS–RADAU RULES TO INTEGRATE
THE ELEMENT MASS AND STIFFNESS MATRICES

($\phi$ is the non-dimensional frequency $= \omega / \sqrt{(D/\rho a^4 t)}$)

| Mesh | Mode | 1 point Gauss–Radau $\phi$ | 2 point Gauss–Radau $\phi$ | 3 point Gauss–Radau $\phi$ | 4 point Gauss–Radau $\phi$ |
|------|------|------|------|------|------|
| (a) | 1 | 1·460 | 3·191 | 3·217 | 3·216 |
|     | 2 |       | 9·115 | 9·065 | 9·058 |
|     | 3 |       | 42·076 | 27·071 | 26·426 |
| (b) | 1 | 2·759 | 3·4336 | 3·4344 | 3·4344 |
|     | 2 | 6·474 | 8·6222 | 8·6197 | 8·6194 |
|     | 3 | 8·779 | 21·1792 | 21·5356 | 21·5228 |
|     | 4 | 12·821 | 26·2970 | 26·7654 | 26·7481 |
|     | 5 | 18·489 | 29·7356 | 30·4174 | 30·3765 |
| (c) | 1 | 3·286446 | 3·46697 | 3·46701 | 3·46700 |
|     | 2 | 7·520522 | 8·54947 | 8·549254 | 8·549243 |
|     | 3 | 17·102822 | 21·51732 | 21·52720 | 21·52702 |
|     | 4 | 22·62412 | 26·98304 | 26·99711 | 26·99674 |
|     | 5 | 24·7099 | 31·04874 | 31·06820 | 31·0674 |
|     | 6 | 33·2939 | 53·3863 | 53·4862 | 53·4798 |

**Абстракт**—Простые функции перемещений для изгиба элементов трехугольных пластинок в часне пригодны для статических решений. В настоящей работе используется этот способ для определения частот и сил выпучивания пластинок.

Получена отличная точность в расчетах частоты и можно предусмотреть почти хорошие условия устойчивости, когда исходится из совершенного крупного разделения элемента. Используется численное интегрирование для определения свойств элемента. Это интегрирование позваляет учесть изменение толщины элемента. Рассматриваются некоторые детали способа расчета.

В заключение представляется существенный метод соответственных значений с точки зрения экономии, который допускает хорошее разделение элементов при расчетах собственных значений ограниченого размера.